Journal of Fluorescence (2021) 31:559–567
https://doi.org/10.1007/s10895-020-02679-9

ORIGINAL ARTICLE

Highly Sensitive Fluorescent Probe for Detection of Paraquat Based on Nanocrystals

Zeinab Pourghobadi[1] · Hadis Makanali[1] · Hakimeh Zare[2]

Received: 15 June 2020 / Accepted: 28 December 2020 / Published online: 19 January 2021

Abstract

Paraquat is one of the most toxic materials widely applied in agriculture in most countries. In the present study, a simple, innovative and inexpensive nano biosensor which is based on a thioglycolic acid (TGA) - CdTe@CdS core-shell nanocrystals (NCs) to detect paraquat, is suggested. The NCs based biosensor shows a linear working range of 10–100 nM, and limited detection of 3.5 nM. The proposed sensor that has been well used for the detection and determination of paraquat in natural water samples is collected from corn field and a canal located near to the corn field yielding recoveries as high as 98%. According to our findings, the developed biosensor shows reproducibility and high sensitivity to determine paraquat in natural water samples in which the amount of paraquat has low levels. The suggested method is efficiently applied to paraquat determination in the samples of natural water that are collected from a tap water and a canal located near to the cornfield.

Keywords Detection · Paraquat · Nanocrystals · Fluorescent · Probe · Sensitive

Introduction

Paraquat (1, 1-dimethyl-4, 4-bipyridium dichloride, PQ^{2+}) is a non-selective herbicide that acts quickly; it was proposed to the market back in 50's. It has been used extensively in agriculture to control weeds. Moreover, since it is highly soluble in water, its excessive usage is harmful to the aquatic environment influencing algae, fish, insects, and probable to contaminate drinking, agricultural and ground waters [1]. Also, PQ^{2+} is easily absorbed into the skin, respiratory tract, and digestive tract resulting in organ damage or even death, it also causes heart, kidney and liver diseases.

The toxicity of paraquat is correlated with the reduction of bivalent cation (PQ^{2+}) and a free radical ($PQ^{\bullet+}$) that reacts with oxygen to form a hydrogen peroxide (H_2O_2), superoxide radical (O^{2-}), and a hydroxyl radical [2, 3]. These radicals are unstable and highly reactive and can easily enter the cell membrane wall, and proteins to cause many diseases, including Parkinson's [4].

As such, some countries have banned it [5, 6]. Yet, since it is relatively cheap and highly efficient, it cannot be replaced by new alternatives in the near future. Thus, its illegal usage should be predicted as its legal usage has been already reported in some countries. This being the case, large-scale application of paraquat is going to be an ongoing problem. Due to its high level of toxicity to mammals and humans, even at low concentrations, the quantitative measurement of the residues of these compounds is very important [7, 8]. Thus, it is highly important to develop some reliable approaches for its detection with high sensitivity and selectivity. Numerous approaches have been already proposed to analyze paraquat including; gas chromatography [9], spectrophotometry [10], liquid chromatography [11], electrochemistry [12], flow injection analysis [13], fluorimetry [5], mass spectrofluorometric method [14], and electrophoresis systems [15, 16]. Although these introduced methods can be efficient for paraquat determination with high sensitivity and selectivity, they are often either instable or expensive with time-consuming preparation steps. Therefore, developing alternative methods, which are highly sensitive, simple, and not costly for detection of paraquat are highly desirable. Recently, optical biosensors have attracted considerable attention because of their applications

✉ Zeinab Pourghobadi
zpourghobadi@gmail.com; zpourghobadi@khoiau.ac.ir

[1] Department of Chemistry, Khorramabad Branch, Islamic Azad University, Khorramabad, Iran

[2] Physics Department, Faculty of Science, Yazd University, P.Box 89195_714, Yazd, Iran

in the fields of environmental monitoring [17–19] biomedical diagnostic [20, 21], food safety [22], and daily healthcare [23].

Fluorescence nanocrystals are new semiconductor nanoparticles that are smaller than the exciton Bohr radius [24]. Compared with fluorescent organic materials, and dye molecules, NCs have excellent physical and chemical properties, including high quantum yield (QY), narrow emission peaks, symmetric emission, broad absorption bands, considerable resistance to photobleaching, suitable to photo-stability, great resistance to photo- and chemical degradation and modifiable emission spectra as well as broad absorption ranging from the ultraviolet (UV) to infrared (IR) region [20, 25, 26].

In the past decade, NCs have been used extensively in medicine for bio tracking of drug molecules [27], bio imaging [28–30], drug delivery [31, 32], antimicrobial deterrence [33], gene delivery [34], photodynamic therapy [35], sensors [36, 37] and bio sensing [38, 39].

Most 'core- only' NCs show an emission blinking behavior, and the fluorescence intensity switching between ON- and OFF-states that restrict their uses significantly. The 'core- only' NCs are described by a low PL QY [40] and a restricted resistance to photobleaching; besides, their PL intensities are simply influenced by charges and free radicals in their peripheral environment. To tackle with these problems, an effective strategy was developed to create core/shell hetero structure systems through coating the core with a protecting shell made from different semiconductor material. The shell should boost the QY, the overall optical features and photo stability of the NCs [26, 40, 41].

Most of sensor applications are in aqueous media where the presence of hydrophilic ligands on the surface of the NCs is necessary. Various types of different ligands, dihydrolipoic acid (DHLA) [42], N-acetyl L-cysteine(N-AC) [43, 44], 3-mercaptopropionic acid (MPA) [45], glutathione (GSH) [39] and thioglycolic acid (TGA) [46, 47] or the coating of the NCs with polymeric materials [48] and silicon oxide films [49] have been employed for surface modification of NCs.

Up to now, several studies have synthesized II-VI semiconductor NCs, particularly aqueous fluorescence NCs for sensing applications. CdTe NCs are the key kind of semiconductor NCs. It is possible to boost the fluorescence efficiency and photostability of CdTe NCs by selecting the appropriate ligand such as TGA and epitaxy development of the cadmium sulfide shell on the core surface. The present study aims to develop a novel biosensing to detect paraquat based on TGA cadmium telluride/cadmium sulfide NCs (CdTe/CdS -NCs), as a fluorescent probe, by the aggregation-based fluorescence property. This novel optical biosensor is highly sensitive with quick response in the detection of paraquat. It is also capable of detecting very low concentrations of paraquat with no pre-concentration steps.

Experimental

Materials and Reagents

TGA and sodium borohydride ($NaBH_4$) were bought from Merck Company. Cadmium sulfate ($CdSO_4$), sodium hydroxide (NaOH), Tellurium (Te) powder, thioacetamide (TAA), and Paraquat were gained from Aldrich Company. All chemicals were employed without further purification.

Using a Philips X'Pert Pro MPD system, powder X-ray diffraction (PXRD) pattern of NCs was recorded at room temperature. A FEI Tecnai G2F30 electron microscope was applied for transmission electron-microscopy (TEM). G9800A Agilent fluorescence spectrophotometer was used for measurement of fluorescence spectra (FL) of NCs-biosensor under atmospheric condition. Excitation wavelength (λ_{ex}) was 360 nm, with slit widths of 10 nm for emission and excitation.

Preparation of CdTe and CdTe/CdS Core/shell NCs

As formerly mentioned, CdTe NCs was prepared [37, 50]. For this purpose, following the addition of NaBH4 (7.3 mmol) into Te (0.87 mmol) and deionized (DI) water (7 mL) under Ar gas, stirring was applied for 3 h. TGA (3.92 mmol) and CdSO4 (2.4 mmol) were further added into DI water (150 mL). Then, NaOH solution was applied to adjust the pH of the solution to 10.0. Through Ar bubbling, the mixture was allowed to be degassed for 45 min. Next, following the injection of NaHTe solution (NaHTe in 43 mL DI water) into the Cd solution, heating was increased to 100 °C for 10 h. Acetone was used to precipitate the fresh NCs, which was then separated by centrifuging, and ultimately added into water. For growth of CdS shell on the surface of NCs, 2.96 mmol CdSO4 was added into a flask containing CdTe NCs and 8.9 mmol TGA. Afterward, the pH of the sample was adapted to 8.0 using NaOH. TAA was applied as the S precursor (5:1 TAA: Cd) to synthesize the core-shell nanoparticles. Afterward, heating was applied to the mixture to 100 °C. The growth of cadmium sulfide shell (100 °C, 8 h) was carried out under argon gas.

Procedure for Detection of PQ^{2+}

Phosphate buffered saline solution (PBS) with pH = 9 was used to prepare all solutions. PQ^{2+} was diluted to proper concentrations. 100 μL of TGA CdTe/CdS NCs (210 μM) were dispersed in 10 mL of buffer solution. 100 μL of NCs was moved into a calibrated test tube, and then PQ2 + solution was added to tube. Buffer solution was added to the tube to reach the final volume to 5 mL. Next, stirring was applied for 150 s. Afterwards, the fluorescence spectra of prepared samples were measured (500 to 700 nm). In this study, different concentrations of PQ^{2+} (10–200 nM) and CdTe/CdS core/shell NCs (100 μL) were used.

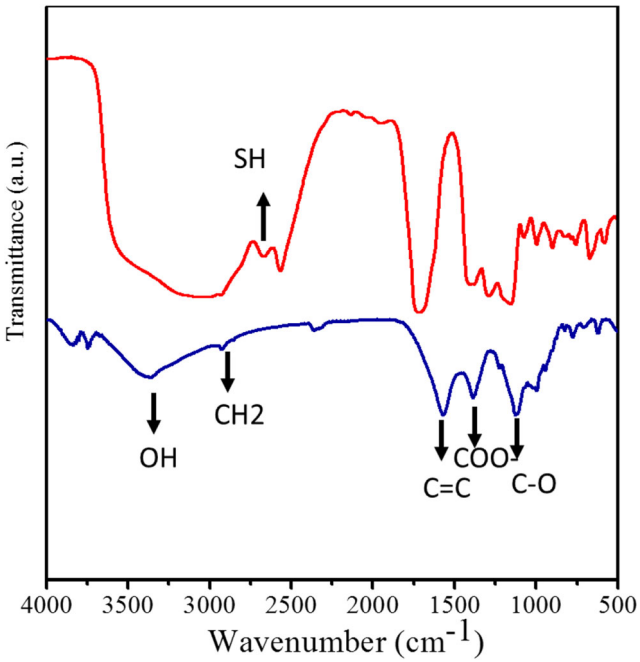

Fig. 1 FT-IR spectra of TGA Ligand and TGA CdTe/CdS- NCs

Water Samples

Real samples were collected from tap water and a canal located near to a corn field, vision area in Khorramabad 10 days after application, which may become polluted by herbicides applied for weed control. Water samples at the temperature below 4 °C were kept and filtered through filters with pore size of 200 nm before analysis.

Results and Discussion

As shown in Fig. 1, the FT-IR spectrum of free TGA shows S-H stretching peaks at ~2568 $cm^{-1}$and 2667 cm^{-1}, the C-O bond at 1150 cm-1 and C = O peak at 1715 cm^{-1}. In the FT-IR spectrum of the TGA CdTe/CdS NCs, the S–H stretching vibration peak was not observed at about 2500–2700 cm^{-1}. This result indicates that the stretched vibration mode disappears because S-H group is covalently bound on the surface of NCs via Cd-S. In both cases, a broad absorption band seen around 3400 cm^{-1} was consigned to O–H vibrations of the aqueous solution. A change in the CH_2 vibrations at 2924 cm^{-1} was observed by NCs when compared with the pure TGA. Also, the absorption peaks at 1715 and 1405 cm^{-1} are due to stretching vibration of C = O and carboxyl groups (-COO-) in the FT-IR spectrum of TGA ligand, and in TGA CdTe/CdS NCs. This absorption peaks shifted to 1516 and 1380 cm^{-1}, respectively. Therefore, these results indicate that TGA are connected to the surface of CdTe/CdS NCs. This coating improves the solubility of the CdTe/CdS NCs in water and prevents their agglomeration. Therefore, the remove of the S-H peak provided the evidence of the formation of S–Cd complex and confirmed TGA that had been bound to the surface of NCs.

The high magnification of HRTEM (High-resolution transmission electron microscopy) image of CdTe/CdS core shell NCs is indicated in Fig. 2a. nearly spherical and monodispersed NCs with average particle size of ~3.5 nm can be seen.

The PXRD patterns of CdTe and CdT/CdS core/shell NCs are depicted in Fig. 2b. The main diffraction peaks of cubic phase CdTe- NCs are located at 24.9°, 40.4° and 46.9°for (111), (220), and (311) crystal planes, respectively (JCPDS card no.150,770) [51-53]. It is obvious that no distinguished peaks of CdS were detected from the PXRD pattern. Moreover, the diffraction peaks of CdTe/CdS NCs (25.9°, 43.8° and 51.6°) shift to somewhat larger diffraction angles. Moreover, the diffraction peaks are quite similar to that of CdTe NCs in terms of the shape indicating the epitaxial development of the CdS shell over the CdTe core NCs [44]. The standard size of NCs is calculated from Debye Scherrer ‘s formula [36]:

$$D = \frac{k\lambda}{\beta\cos(\theta)}$$

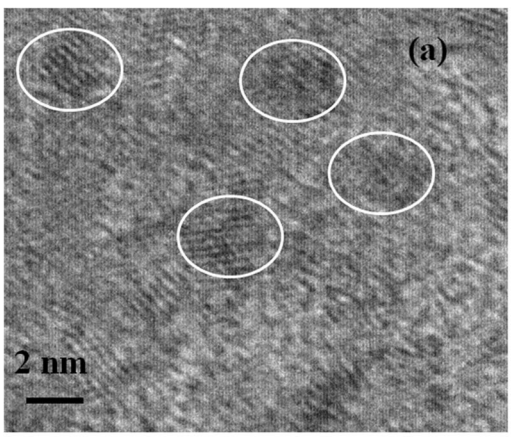

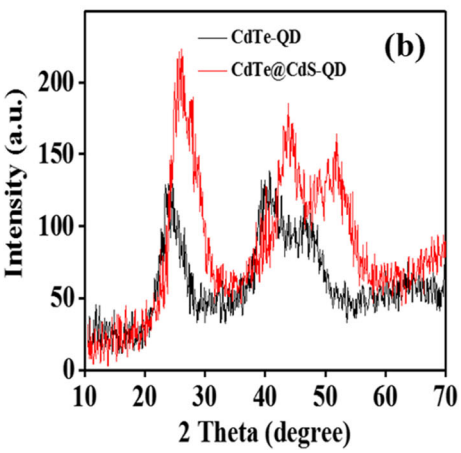

Fig. 2 **a** HR-TEM image of CdTe/CdS core/shell NCs (Scale bar is 2 nm) and **b** PXRD spectra of CdTe and CdTe/CdS core/shell NCs

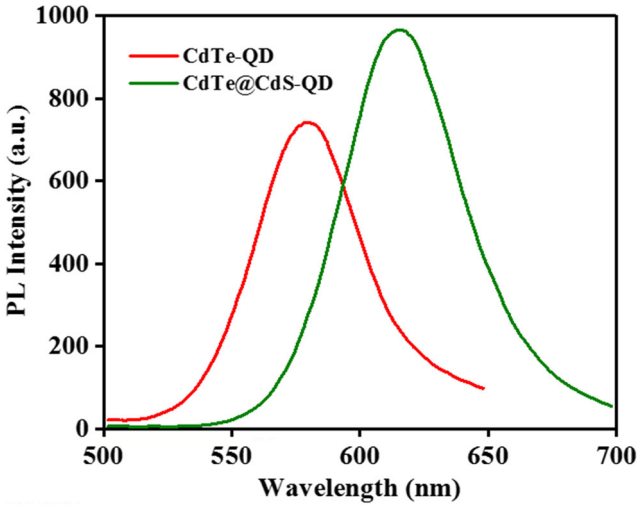

Fig. 3 Fluorescence spectra of CdTe/CdS core/shell and CdTe NCs

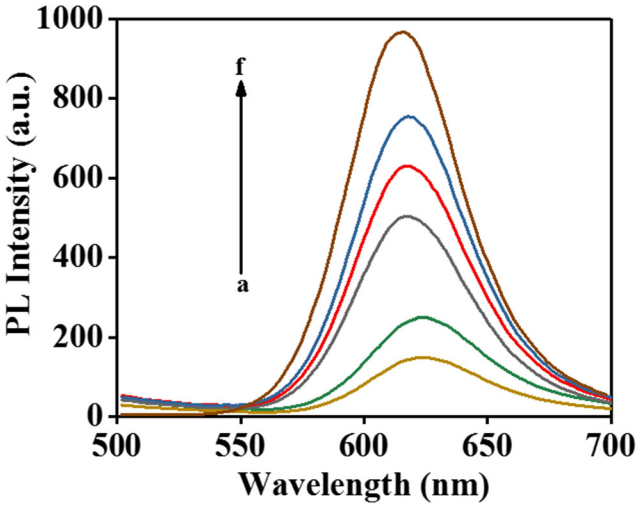

Fig. 5 **a** Fluorescence spectra of TGA CdTe/CdS core/shell NCs by different concentrations of NCs (4.2–42 nM) (pH = 9, 25 °C)

that, D is the average size of the NCs, k is a structural constant (k ≅ 1 for the particles with spherical shape [36]), β is the full width at half maximum of the peak, θ is the Bragg angle, and λ is the wavelength of Cu Kα radiation (1.54 Å).

The average size of the CdTe/CdS QDs is estimated to be ~ 3.6 nm".

Fluorescence spectra of CdTe/CdS core/shell and CdTe NCs were recorded (500–700 nm). As Fig. 3 shows, the development of CdS shell on the surface of core-NCs decreased the surface traps leading to enhanced fluorescence efficiency. The shift of fluorescence spectrum to larger wavelengths confirmed the formation of core/shell structure.

Effect of solution pH on the sensor

The influence of pH (5.0–10.0) on the fluorescence spectrum of TGA-CdTe/CdS NCs in the presence of PQ^{2+} was studied since it affects the performance of the sensor. Figure 4 shows the plots that are relative fluorescence intensity F0/F versus pH and in which F0 and F are the fluorescence intensities of NC solution before and after the addition of PQ^{2+}, respectively.

TGA-CdTe/CdS core/shell NCs are unstable when the solution pH is less than 5, therefore pHs more than 5 is selected. The relative fluorescence intensity of F0/F gradually increases with the increase of pH. Hence, pH 9.0 was selected as the optimal pH for determining PQ^{2+} by the proposed method because pKa of the–COOH group in thioglycolic acid is 3.6, thus, the zeta potential of the TGA CdTe/CdS-NCs was negative at pH 9.0.

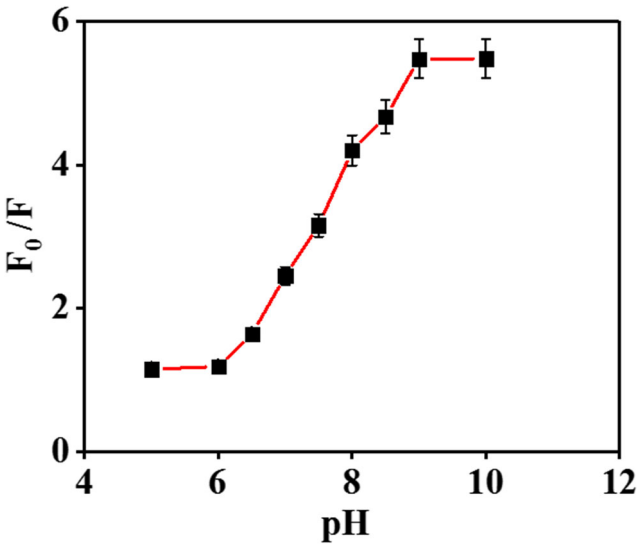

Fig. 4 The influence of the pH on the fluorescence spectrum of TGA CdTe/CdS core/shell NCs (42 nM) in the presence of 100 nM PQ^{2+} (pH = 9, 25 °C)

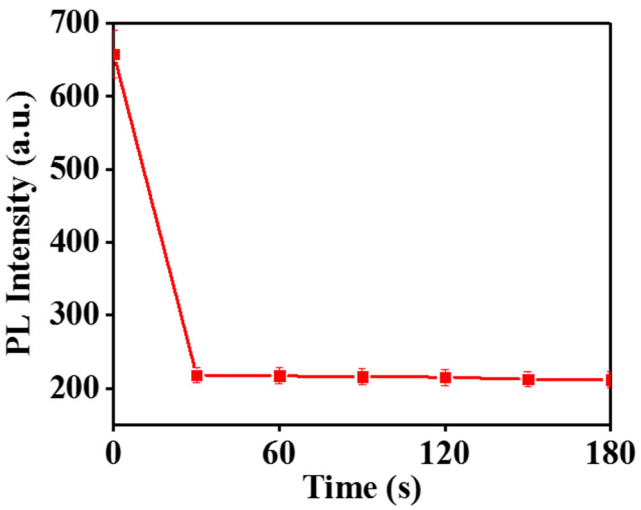

Fig. 6 The influence of the incubation time with PQ^{2+} (100 nM) on the CdTe/CdS core/shell NCs fluorescence signal at pH = 9

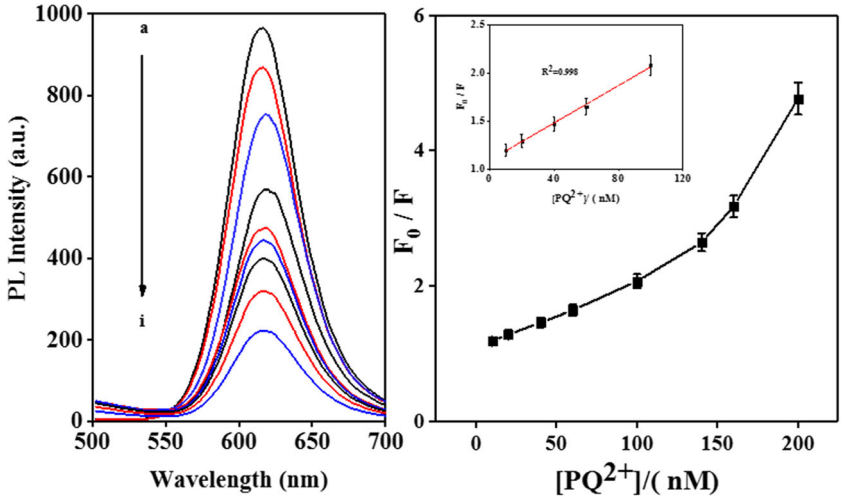

Fig. 7 Fluorescence spectra of the TGA-capped CdTe/CdS- QDs probe in the presence of PQ^{2+} at different concentrations (from top to bottom: 0, 10.0, 20.0, 40.0, 60.0.0, 80.0,100, 140, 160, and 200 nM), and the corresponding calibration plot

Since, PQ^{2+} is a well-known electron transfer quenching agent (acceptor), and also TGA CdTe/CdS NCs (donor) have negative charge at pH = 9, the electrostatic interaction between the NCs and PQ^{2+} and electron transfer quenching occurs and the fluorescence signal is decreased. There was a 4 nm red shift in the emission peak. This incident proves that the addition of PQ^{2+} continues with the reduction of the surface charge of NCs. Electrostatic repulsive force of the NCs decreases, which leads to the agglomeration NCs. As such, the red shifts of the CdTe/CdS NCs fluorescence emission have been observed [55, 56].

Effect of TGA CdTe/CdS NCs

The effect of TGA CdTe/CdS NCs concentration on fluorescence spectrum was thoroughly studied (Fig. 5). The fluorescence intensity of the sample was enhanced with the increasing concentration of TGA CdTe/CdS NCs in the range 4.2 to 42 nM. As shown in Fig. 5, by increasing the concentration of TGA CdTe/CdS NCs, the fluorescence emission increased, consequently, the concentration of 42 nM was chosen as the optimal concentration of NCs.

The Effect of Incubation Time

To assess the stability of the fluorescence probe sensing system, we investigated the time-dependence of the fluorescence quenching of the TGA CdTe/CdS NCs. The time-dependent fluorescence quenching of TGA CdTe/CdS NCs was studied under optimum conditions (pH = 9, 42n M NCs) and in the presence of PQ^{2+} (100 nM) (Fig. 6). The experimental results revealed that the reaction finished within 30 s and the fluorescence intensity was stable more than 180 s, which indicated that the TGA CdTe/CdS NCs displayed higher stability and fast sensing of PQ^{2+}. More experiments were conducted using the time scale of 30 s.

Effect of the Concentration of PQ^{2+} on the Quenching of Fluorescence Signal

Under the optimal conditions described above, the impact of PQ^{2+} concentration on the fluorescence signal of CdTe/CdS core/shell NCs was examined in detail. According to the results, the fluorescence intensity was reduced by increased concentration of PQ^{2+} in the range of 10–200 nM.

The Stern–Volmer equation was applied to investigate the relationship between quenching efficiency of NCs and concentration of PQ^{2+} [36, 39, and 50]:

$$F0/F. = 1 + Ks\ [PQ^{2+}] \quad (1)$$

Where F_0 shows the fluorescence intensity at 608 nm in the absence of PQ^{2+} and F is fluorescence intensity of sample after adding of PQ^{2+}, respectively: Ks denotes Stern Volmer

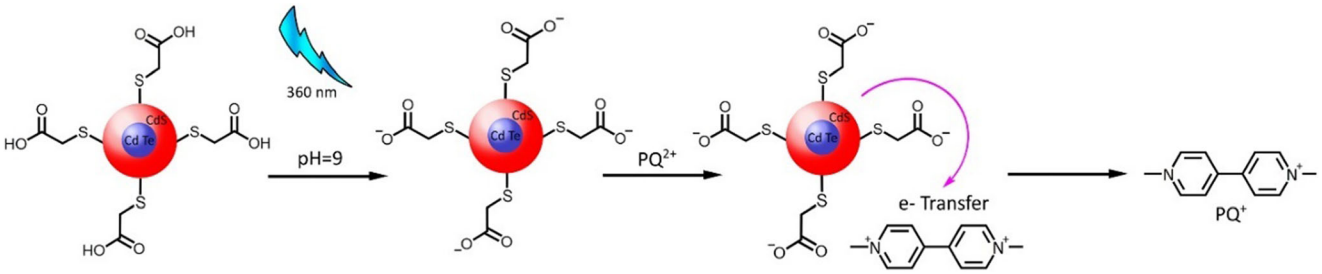

Scheme 1 An illustration of the sensor PQ^{2+} detection through the fluorescence quenching mechanism

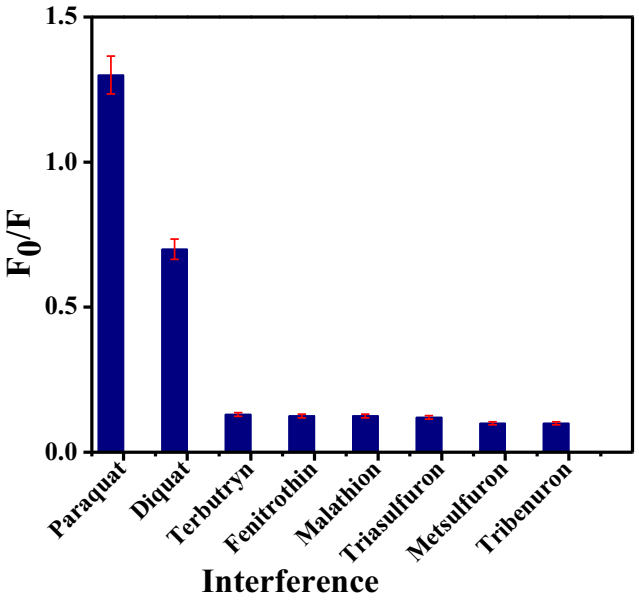

Fig. 8 The selectivity of TGA CdTe/CdS core/shell NCs probe to various types of pesticides fluorescence intensity (F0/F) of the system under optimum conditions

quenching constant, and [PQ^{2+}] is the concentration of quencher (PQ^{2+}). Based on equation Stern-Volmer, a likely mechanism for quenching could be recommended in the sensing process. If one kind of quenching mechanism is observed by the quenching process, then, the Eq. 1 is sufficient to illustrate the quenching process. According to the Stern–Volmer plot, F_0/F vs. PQ^{2+} concentration is linear at the lower concentration of PQ^{2+} while it diverges from linearity by winding up in higher concentration (Fig. 7). This marks the existence of both static and dynamic quenching of the fluorescence in the mechanism of interaction [53]. A vast range of processes can lead to the fluorescence quenching including excited state reactions, complex formation energy transfer, complex formation and collisional quenching. The processes of collisional quenching and complex formation are often referred to as quenching respectively. The result of this study displays that both static and dynamic quenching are present in this system. Yet, both static and dynamic quenching requires molecular contact between the fluorophore and the quencher. In this case of collisional quenching, electrostatic interactions between the positive charged segment of PQ^{2+} because of heterocyclic systems and carboxyl groups in TGA NCs (pKa = 3.6 for TGA) led to the adsorption of PQ^{2+} as strong acceptor on TGA causing its fluorescence to be quenched [14, 50, 54]. After introducing the PQ^{2+} to the probe solution, electrons are transferred between the NCs and PQ^{2+} that lead to the formation of the radicals and a reaction with molecular oxygen (Scheme 1).

Also, the presence of aromatic groups in the structure of paraquat and the π- π stacking interaction in its structure with NCs lead to a decrease in the intensity of fluorescence, which is called a phenomenon of fluorescence resonance energy transfer (FRET) [14].

According to the results, biosensor response in the range of 10–100 nM was linear with a correlation coefficient of 0.998. The linear regression equation was described as F0/F = 1.09 + 0.0097[PQ^{2+}] R2= (R2 = 0.998) (Fig. 7).

According to the results, the fluorescence intensity was directly related to the PQ^{2+} concentration within the mentioned range of a detection limit of 3.5 nM (S/N = 3). This shows that TGA CdTe/CdS NCs were highly sensitive for targeted PQ^{2+} detection. PQ^{2+} Limit of Detection was evaluated based on the definition of 3σ/s, in which σ and s are the standard deviation of the blank (n = 5) and the calibration graph slope in the respective order. Under the optimal conditions, the value of relative standard deviation for 5 replicates of 10 nM of PQ^{2+} was 2.45%.

It has been shown that the practical application of a sensor is dependent on its selectivity.

To assess the selectivity of the suggested NC-biosensor, under the optimal conditions, we have also investigated the influence of some metal ions such as 5 mM Ba^{2+}, 2 mM Mg^{2+}, 10 mM Na^{+}, 2 mM Ca^{2+}, and anion various substances for instance: 2 mM ClO^{-}, 10 mM NO_3^{-}, 10 mM Cl^{-}, fluorescence intensity of NCs stayed unchanged, signifying the electrostatic interaction between mentioned cations with NCs was not strong. Afterwards, the fluorescence of NCs was quenched by the addition of 20 nM of PQ^{2+} into NCs solution.

To further verify the applicability of the fluorescence NC-biosensor for detection PQ^{2+} in practical applications, we have also examined the effect of 100 nM with different substances

Table 1 Recovery test for the detection of PQ^{2+} samples (n = 5)

Sample	Added (nM)	Found (nM)	Recovery (%)
Tap water	10	9.9±0.5	99
Tap water	100	9.8±0.4	98
Canal water	10	10.3±0.6	103
Canal water	100	102.3±0.3	102.3

* Canal water: water collected from canal near to the corn field

Table 2 Comparing the results of the proposed method with similar reports

Method	Linear range (μM)	Detection limit (μM)	RSD%	Refrance
SWV	0.05–0.6	0.0022	-	[12]
Fluorescence	1.0–20	0.2	-	[14]
Fluorescence	0.09–5.83	0.039	2.5	[54]
AsDPVs	0.1–10	0.068		[57]
Fluorescence	10–100 nM	0.0035	2.45	This work

*DPV: Differential pulse voltammetry, SWV: Square wave voltammetry

for instance diquat, terbutryn, fenitrothion, malathion, triasulfuron, metasulfuron and tribenuron in the presence of 20 nM of PQ^{2+}. As shown in Fig. 8 the fluorescence intensity ratio F_0/F had no obvious change.

According to the results, NCs-based sensor is highly selective towards PQ^{2+}. The high selectivity against competitive cations and different substances good linearity as well as simple sensing mechanism shows its possible application to measure PQ^{2+} in natural water sample reliably and endurably.

Real Sample Analysis

To confirm the practicability of the sensor, the prepared biosensor was also applied to determine PQ^{2+} with the standard addition methods in the natural water samples. Table 1 shows the results. The measured recoveries were as high as 98% (n = 5) with the RSD less than 10.0% showing the sensor is precise and reliable which could be used to quantify PQ^{2+} in real samples.

Conclusions

In the present study, a novel nanosensor is fabricated and is introduced as a simple fluorimetric sensor to detect PQ^{2+} detection using TGA CdTe/CdS-NCs. Since, PQ^{2+} is a significant agent acceptor and TGA CdTe/CdS-NCs is an agent donor (pH = 9, therefore, the NCs and PQ^{2+} interact electrostatically and transfer quenching occurs leading to reduced fluorescence signal. We were able to apply the suggested optical biosensor successfully to detect PQ^{2+} in real samples. Table 2 compares the figures of the present approach with other reported approaches to detect PQ^{2+}. According to Table 2, the detection limit and dynamic range value of the present biosensor is lower or comparable with different methods for measuring PQ^{2+}. Consequently, the proposed method presents a clear advantage in terms of sensitivity and selectivity as the proposed sensor is a promising tool for the determination of PQ^{2+} in real samples.

Acknowledgements The authors greatly appreciate the financial support to the present study by the Khorramabad Branch of Islamic Azad University, Lorestan Province, Iran.

Author Contributions The all authors confirm that the manuscript have been read and approved by all named authors. We further confirm that the order of authors listed in the manuscript has been approved by all of us.

Data Availability Not applicable.

Compliance with Ethical Standards

Competing Interests The authors declare that they have no conflict of interest.

Code Availability Not applicable.

References

1. Siangproh W, Somboonsuk T, Chailapakul O, Songsrirote K (2017) Novel colorimetric assay for paraquat detection on-silica bead using negatively charged silver nanoparticles. Talanta 174: 448–453. https://doi.org/10.1016/j.talanta.2017.06.045
2. dos Santos LBO, Infante CMC, Masini JC (2010) Development of a sequential injection–square wave voltammetry method for determination of paraquat in water samples employing the hanging mercury drop electrode. Anal Bioanal Chem 396:1897–1903. https://doi.org/10.1007/s00216-009-3429-x
3. Chuntib P, Themsirimongkon S, Saipanya S, Jakmunee J (2017) Sequential injection differential pulse voltammetric method based on screen printed carbon electrode modified with carbon nanotube/Nafion for sensitive determination of paraquat. Talanta 170:1–8. https://doi.org/10.1016/j.talanta.2017.03.073
4. Gao R, Choi N, Chang S-I et al (2010) Highly sensitive trace analysis of paraquat using a surface-enhanced Raman scattering microdroplet sensor. Anal Chim Acta 681:87–91. https://doi.org/10.1016/j.aca.2010.09.036
5. Sun S, Li F, Liu F et al (2015) Fluorescence detecting of paraquat using host-guest chemistry with cucurbit[8]uril. Sci Rep 4:3570. https://doi.org/10.1038/srep03570
6. de Figueiredo-Filho LCS, Baccarin M, Janegitz BC, Fatibello-Filho O (2017) A disposable and inexpensive bismuth film minisensor for a voltammetric determination of diquat and paraquat pesticides in natural water samples. Sensors Actuators B Chem 240:749–756. https://doi.org/10.1016/j.snb.2016.08.157
7. Onyon LJ, Volans GN (1987) The epidemiology and prevention of paraquat poisoning. Hum Toxicol 6:19–29. https://doi.org/10.1177/096032718700600104
8. Tu J, Xiao L, Jiang Y et al (2015) Near-infrared fluorescent turn-on detection of paraquat using an assembly of squaraine and surfactants. Sensors Actuators B Chem 215:382–387. https://doi.org/10.1016/j.snb.2015.04.015
9. Geng P, Jinzhang C, Lijing Z, Mengzhi X, Zezheng L, Jing Z, Zhiyi W, Xianqin Wang CW, Ma J (2017) Liver tissue metabonomics in rat after acute paraquat poisoning gas chromatography-mass spectrometry. Int J Clin Exp Med 10:937–943
10. Faust SD, Hunter NE (1965) Chemical methods for the detection of aquatic herbicides. J Am Water Works Assoc 57:1028–1037. https://doi.org/10.1002/j.1551-8833.1965.tb01494.x
11. Gill R, Qua SC, Moffat AC (1983) High-performance liquid chromatography of paraquat and diquat in urine with rapid sample preparation involving ion-pair extraction on disposable cartridges of octadecyl-silica. J Chromatogr A 255:483–490. https://doi.org/10.1016/S0021-9673(01)88303-5
12. Tomková H, Sokolová R, Opletal T et al (2018) Electrochemical sensor based on phospholipid modified glassy carbon electrode - determination of paraquat. J Electroanal Chem 821:33–39. https://doi.org/10.1016/j.jelechem.2017.12.048
13. Jain A, Verma KK, Townshend A (1993) Determination of paraquat by flow-injection spectrophotometry. Anal Chim Acta 284: 275–279. https://doi.org/10.1016/0003-2670(93)85311-7
14. Zhao Z, Zhang F, Zhang Z (2018) A facile fluorescent "turn-off" method for sensing paraquat based on pyranine-paraquat interaction. Spectrochim Acta Part A Mol Biomol Spectrosc 199:96–101. https://doi.org/10.1016/j.saa.2018.03.042
15. Wigfield YY, McCormack KA, Grant R (1993) Simultaneous determination of residues of paraquat and diquat in potatoes using high-performance capillary electrophoresis with a ultraviolet detection. J Agric Food Chem 41:2315–2318. https://doi.org/10.1021/jf00036a018
16. Núñez O, Moyano E, Galceran M (2002) Solid-phase extraction and sample stacking–capillary electrophoresis for the determination

of quaternary ammonium herbicides in drinking water. J Chromatogr A 946:275–282. https://doi.org/10.1016/S0021-9673(01)01562-X
17. Ensafi AA, Kazemifard N, Rezaei B (2015) A simple and rapid label-free fluorimetric biosensor for protamine detection based on glutathione-capped CdTe quantum dots aggregation. Biosens Bioelectron 71:243–248. https://doi.org/10.1016/j.bios.2015.04.015
18. Ding L, Ruan Y, Li T et al (2018) Nitric oxide optical fiber sensor based on exposed core fibers and CdTe/CdS quantum dots. Sensors Actuators B Chem 273:9–17. https://doi.org/10.1016/j.snb.2018.06.012
19. Dong L-Y, Wang L-Y, Wang X-F et al (2016) Development of fluorescent FRET probe for determination of glucose based on β-cyclodextrin modified ZnS-quantum dots and natural pigment 3-hydroxyflavone. Dye Pigment 128:170–178. https://doi.org/10.1016/j.dyepig.2016.01.032
20. Ding L, Zhang B, Xu C et al (2016) Fluorescent glucose sensing using CdTe/CdS quantum dots–glucose oxidase complex. Anal Methods 8:2967–2970. https://doi.org/10.1039/C5AY03205A
21. Algar WR, Krull UJ (2008) Quantum dots as donors in fluorescence resonance energy transfer for the bioanalysis of nucleic acids, proteins, and other biological molecules. Anal Bioanal Chem 391:1609–1618. https://doi.org/10.1007/s00216-007-1703-3
22. Zhang M, Cao X, Li H et al (2012) Sensitive fluorescent detection of melamine in raw milk based on the inner filter effect of Au nanoparticles on the fluorescence of CdTe quantum dots. Food Chem 135:1894–1900. https://doi.org/10.1016/j.foodchem.2012.06.070
23. Shen S-L, Zhang X-F, Ge Y-Q et al (2018) A novel ratiometric fluorescent probe for the detection of HOCl based on FRET strategy. Sensors Actuators B Chem 254:736–741. https://doi.org/10.1016/j.snb.2017.07.158
24. Frigerio C, Ribeiro DSM, Rodrigues SSM et al (2012) Application of quantum dots as analytical tools in automated chemical analysis: A review. Anal Chim Acta 735:9–22. https://doi.org/10.1016/j.aca.2012.04.042
25. Bagheri Z, Ehtesabi H, Hallaji Z et al (2018) Investigation the cytotoxicity and photo-induced toxicity of carbon dot on yeast cell. Ecotoxicol Environ Saf 161:245–250. https://doi.org/10.1016/j.ecoenv.2018.05.071
26. Foubert A, Beloglazova NV, Rajkovic A et al (2016) Bioconjugation of quantum dots: Review & impact on future application. TrAC Trends Anal Chem 83:31–48. https://doi.org/10.1016/j.trac.2016.07.008
27. Elmizadeh H, Soleimani M, Faridbod F, Bardajee GR (2018) Fabrication and optimization of a sensitive tetracycline fluorescent nano-sensor based on oxidized starch polysaccharide biopolymer-capped CdTe/ZnS quantum dots: Box–Behnken design. J Photochem Photobiol A Chem 367:188–199. https://doi.org/10.1016/j.jphotochem.2018.08.021
28. Karakoti AS, Shukla R, Shanker R, Singh S (2015) Surface functionalization of quantum dots for biological applications. Adv Colloid Interface Sci 215:28–45. https://doi.org/10.1016/j.cis.2014.11.004
29. Banerjee A, Grazon C, Nadal B et al (2015) Fast, efficient, and stable conjugation of multiple DNA strands on colloidal quantum dots. Bioconjug Chem 26:1582–1589. https://doi.org/10.1021/acs.bioconjchem.5b00221
30. Banerjee A, Grazon C, Pons T et al (2017) A novel type of quantum dot–transferrin conjugate using DNA hybridization mimics intracellular recycling of endogenous transferrin. Nanoscale 9:15453–15460. https://doi.org/10.1039/C7NR05838A
31. Wang J, Jiang P, Gao L et al (2013) Unique self-assembly properties of a bridge-shaped protein dimer with quantum dots. J Nanoparticle Res 15:1914. https://doi.org/10.1007/s11051-013-1914-9
32. Su X, Chan C, Shi J et al (2017) A graphene quantum dot@Fe 3 O 4 @SiO 2 based nanoprobe for drug delivery sensing and dual-modal fluorescence and MRI imaging in cancer cells. Biosens Bioelectron 92:489–495. https://doi.org/10.1016/j.bios.2016.10.076
33. Jin T, Sun D, Su JY et al (2009) Antimicrobial efficacy of zinc oxide quantum dots against Listeria monocytogenes, Salmonella Enteritidis, and Escherichia coli O157:H7. J Food Sci 74:M46–M52. https://doi.org/10.1111/j.1750-3841.2008.01013.x
34. Zhou J, Deng W, Wang Y et al (2016) Cationic carbon quantum dots derived from alginate for gene delivery: One-step synthesis and cellular uptake. Acta Biomater 42:209–219. https://doi.org/10.1016/j.actbio.2016.06.021
35. Samia ACS, Chen X, Burda C (2003) Semiconductor quantum dots for photodynamic therapy. J Am Chem Soc 125:15736–15737. https://doi.org/10.1021/ja0386905
36. Feizi S, Zare H, Hoseinpour M (2018) Investigation of dosimetric characteristics of a core–shell quantum dots nano composite (CdTe/CdS/PMMA): fabrication of a new gamma sensor. Appl Phys A 124:420. https://doi.org/10.1007/s00339-018-1837-5
37. Zare H, Ghalkhani M, Akhavan O et al (2017) Highly sensitive selective sensing of nickel ions using repeatable fluorescence quenching-emerging of the CdTe quantum dots. Mater Res Bull 95:532–538. https://doi.org/10.1016/j.materresbull.2017.08.015
38. Li Y, Sun L, Liu Q et al (2016) Photoelectrochemical CaMV35S biosensor for discriminating transgenic from non-transgenic soybean based on SiO2@CdTe quantum dots core-shell nanoparticles as signal indicators. Talanta 161:211–218. https://doi.org/10.1016/j.talanta.2016.08.047
39. İnal EK (2020) A fluorescent chemosensor based on schiff base for the determination of Zn2+, Cd2 + and Hg2+. J Fluoresc 30:891–900. https://doi.org/10.1007/s10895-020-02563-6
40. Nirmal M, Dabbousi BO, Bawendi MG et al (1996) Fluorescence intermittency in single cadmium selenide nanocrystals. Nature 383:802–804. https://doi.org/10.1038/383802a0
41. Marandi M, Emrani B, Zare H (2017) Synthesis of highly luminescent CdTe/CdS core-shell nanocrystals by optimization of the core and shell growth parameters. Opt Mater (Amst) 69:358–366. https://doi.org/10.1016/j.optmat.2017.04.058
42. Yu Y, Zhang K, Li Z, Sun S (2012) Synthesis and luminescence characteristics of DHLA-capped PbSe quantum dots with biocompatibility. Opt Mater (Amst) 34:793–798. https://doi.org/10.1016/j.optmat.2011.11.008
43. Wu T, He K, Zhan Q et al (2015) Partial protection of N-acetylcysteine against MPA-capped CdTe quantum dot-induced neurotoxicity in rat primary cultured hippocampal neurons. Toxicol Res (Camb) 4:1613–1622. https://doi.org/10.1039/C5TX00127G
44. Chen Y, Chen Z, He Y et al (2010) L-cysteine-capped CdTe QD-based sensor for simple and selective detection of trinitrotoluene. Nanotechnology 21:125502. https://doi.org/10.1088/0957-4484/21/12/125502
45. Shankara Narayanan S, Sinha SS, Verma PK, Pal SK (2008) Ultrafast energy transfer from 3-mercaptopropionic acid-capped CdSe/ZnS QDs to dye-labelled DNA. Chem Phys Lett 463:160–165. https://doi.org/10.1016/j.cplett.2008.08.057
46. Jhonsi MA, Renganathan R (2010) Investigations on the photoinduced interaction of water soluble thioglycolic acid (TGA) capped CdTe quantum dots with certain porphyrins. J Colloid Interface Sci 344:596–602. https://doi.org/10.1016/j.jcis.2010.01.022
47. Khan S, Carneiro LSA, Vianna MS et al (2017) Determination of histamine in tuna fish by photoluminescence sensing using thioglycolic acid modified CdTe quantum dots and cationic solid phase extraction. J Lumin 182:71–78. https://doi.org/10.1016/j.jlumin.2016.09.041

48. Fernández-Argüelles MT, Costa-Fernández JM, Pereiro R, Sanz-Medel A (2008) Simple bio-conjugation of polymer-coated quantum dots with antibodies for fluorescence-based immunoassays. Analyst 133:444. https://doi.org/10.1039/b802360n
49. Shiohara A, Hanada S, Prabakar S et al (2010) Chemical reactions on surface molecules attached to silicon quantum dots. J Am Chem Soc 132:248–253. https://doi.org/10.1021/ja906501v
50. Pourghobadi Z, Mirahmadpour P, Zare H (2018) Fluorescent biosensor for the selective determination of dopamine by TGA-capped CdTe quantum dots in human plasma samples. Opt Mater (Amst) 84:757–762. https://doi.org/10.1016/j.optmat.2018.08.003
51. Uvarov V, Popov I (2007) Metrological characterization of X-ray diffraction methods for determination of crystallite size in nanoscale materials. Mater Charact 58:883–891. https://doi.org/10.1016/j.matchar.2006.09.002
52. Lakowicz JR (2013) Principles of fluorescence spectroscopy. Springer Sci Bus Media, Berlin
53. Matylitsky VV, Dworak L, Breus VV et al (2009) Ultrafast charge separation in multiexcited CdSe quantum dots mediated by adsorbed electron acceptors. J Am Chem Soc 131:2424–2425. https://doi.org/10.1021/ja808084y
54. Li H, Liu J, Yang X (2015) Facile synthesis of glutathione-capped CdS quantum dots as a fluorescence sensor for rapid detection and quantification of paraquat. Anal Sci 31:1011–1017. https://doi.org/10.2116/analsci.31.1011
55. Jenkins R, de Vries JL (1997) An introduction to X-ray powder diffractometryNo Title. NV Philips 36:1128
56. Scherrer PJNGWG (1918) Estimation of the size and internal structure of colloidal particles by means of röntgen. Nachr Ges Wiss Göttingen 2:96–100
57. Ghalkhani M, Maghsoudi S, Saeedi R, Khaloo SS (2019) Ultrasensitive quantification of paraquat using a newly developed sensor based on silver nanoparticle-decorated carbon nanotubes. J Iran Chem Soc 16:1301–1309. https://doi.org/10.1007/s13738-019-01605-6